THE JOURNAL OF PHYSICAL CHEMISTRY Letters

Letter

Cite This: J. Phys. Chem. Lett. 2019, 10, 3516−3524

pubs.acs.org/JPCL

Cation Alloying Delocalizes Polarons in Lead Halide Perovskites

Liujiang Zhou,*[,†,‡] Claudine Katan,[¶] Wanyi Nie,[§] Hsinhan Tsai,[§] Laurent Pedesseau,[∥] Jared J. Crochet,[⊥] Jacky Even,[∥] Aditya D. Mohite,[#] Sergei Tretiak,[‡] and Amanda J. Neukirch*[,‡]

[†]Institute of Fundamental and Frontier Sciences, University of Electronic Science and Technology of China, Chengdu 610054, P. R. China

[‡]Theoretical Physics and Chemistry of Materials, [§]Materials Physics and Application, and [∥]Physical Chemistry and Applied Spectroscopy Division, Los Alamos National Laboratory, Los Alamos, New Mexico 87545, United States

[¶]Univ Rennes, ENSCR, INSA Rennes, CNRS, ISCR - UMR 6226, F-35000 Rennes, France

[⊥]Univ Rennes, INSA Rennes, CNRS, Institut FOTON - UMR 6082, F-35000 Rennes, France

[#]Department of Chemical and Biomolecular Engineering, Rice University, Houston, Texas 77006, United States

Supporting Information

ABSTRACT: Recently, mixed-cation perovskites have promised enhanced performances concerning stability and efficiency in optoelectronic devices. Here, we report a systematic study on the effects of cation alloying on polaronic properties in cation-alloyed perovskites using first principle calculations. We find that cation alloying significantly reduces the polaron binding energies for both electrons and holes compared to pure methylammonium lead iodide ($MAPbI_3$). This is rationalized in terms of crystal symmetry reduction that causes polarons to be more delocalized. Electron polarons undergo large Jahn−Teller distortions (∼15−30%), whereas hole polarons tend to shrink the lattice by ∼5%. Such different lattice distortion footprints could be utilized to distinguish the type of polarons. Finally, our simulations show that Cs, formamidinium (FA), and MA mixtures can effectively minimize polaron binding energy while weakly affecting band gap, in a good agreement with experimental findings. These modeling results can guide future development of halide perovskite materials compositions for optoelectronic applications.

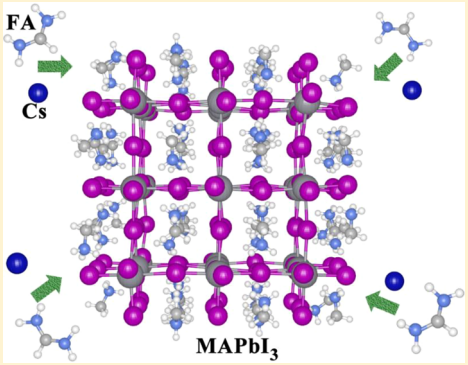

Three-dimensional lead halide perovskites with the general formula $APbX_3$ (where A is a monovalent cation and X = I, Br, or Cl) are composed of earth-abundant elements and are solution processable. These materials have shown promise for various optoelectronic applications while retaining low cost.[1,2] The prototypical halide perovskite, $MAPbI_3$, with a band gap of 1.6 eV,[3] has been successfully utilized as an excellent active material for light harvesting in solar cells with outstanding power conversion efficiency approaching 21%.[4] In fact, solution-processed halide perovskites (HPs) are favorable candidates for a diverse range of applications including photovoltaics, light-emitting diodes,[5,6] hydrogen generation,[7] X-ray and gamma-ray detection,[8,9] spintronics,[10] and sensors.[11] The superb performances of halide perovskites are due to unique photophysical traits, including low carrier effective masses, low electron−hole recombination rates, ambipolar charge transport, high extinction coefficients, and long charge carrier diffusion lengths.[12−14]

Despite these initial demonstrations, the most significant barrier in the progress toward halide perovskite device commercialization is the lack of stability to temperature, oxygen, humidity, and exposure to light.[15−17] Hybrid perovskites are prone to chemical reactions, phase transformations, phase segregation, and other degradation processes under ambient conditions. Numerous strategies, including reducing structural dimensionality,[18,19] chemical makeup,[20,21] antisolvent additive deposition,[22] and defect creation,[23] have been applied to the original $MAPbI_3$ structure in order to achieve a more stable and efficient solar cell material.[24,25] For example, when making A-site substitutions to the lead halide perovskites, various improvements are found. The $FAPbI_3$ perovskite has an advantageous red-shift in bandgap and is less susceptible to thermal degradation compared to its MA equivalent.[25,26] However, it lacks structural stability, and its photoactive α-phase ("black phase") is stable at elevated temperatures (>60 °C).[27] At room temperature, $FAPbI_3$ tends to transform into the nonperovskite δ-phase ("yellow phase").[27] One of the main reasons for decomposition of MA and FA perovskites is the high volatility of the organic cations.[28] Therefore, the all inorganic alternative, $CsPbI_3$, has drawn a lot of consideration.[25,27,29−31] Cs salts are less volatile than their organic counterparts and exhibit excellent thermal stability up to temperatures as high as 300 °C.[29,31−33] Unfortunately, in

Received: April 15, 2019
Accepted: June 7, 2019
Published: June 7, 2019

DOI: 10.1021/acs.jpclett.9b01077
J. Phys. Chem. Lett. 2019, 10, 3516−3524

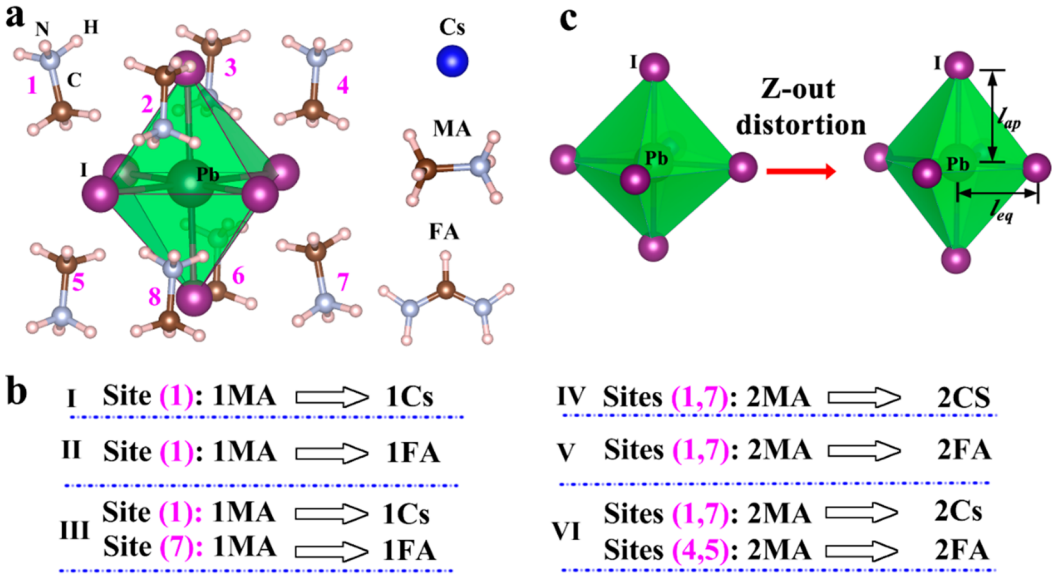

Figure 1. (a) Schematic diagram of a PbI_6 octahedron and the eight surrounding MA molecules. (b) Six substitution models are derived from the basic $MAPbI_3$ cluster with a stoichiometry of $A_{54}Pb_{27}I_{108}$, where A is a mixture of the three cations. These models are denoted as Cs−$MAPbI_3$ (I), FA−$MAPbI_3$ (II), CsFA−$MAPbI_3$ (III), 2Cs−$MAPbI_3$ (IV), 2FA−$MAPbI_3$ (V), and 2(CsFA)−$MAPbI_3$ clusters (VI). The Cs and FA substitutions are considered along a diagonal around the central Pb in order to minimize the net dipole moment. The pink numbers are denoted to mark the sites where the substitutions are performed. (c) Schematic diagram of Jahn−Teller (JT) distortions. The equatorial (l_{eq}) and apical (l_{ap}) bond lengths are also marked.

addition to having a larger band gap, $CsPbI_3$ also suffers for the poor stability of its α-phase and at room temperature tends to transform into another nonperovskite yellow δ-phase.[34] In the absence of pure material exhibiting optimal optoelectronic properties and thermodynamic stability, alloyed materials may offer further structural optimizations. It has been widely demonstrated that double- and/or triple-cation perovskite compositions hold the best solar cell performances. Adding small amounts of MA and Cs to FA perovskites induces crystallization into the photoactive perovskite phase and results in a composition that is more thermally and structurally stable than any of the pure systems.[25,35−42]

In addition, $MAPbI_3$ also suffers from the reversible photodegradation in experiment[43] that was attributed to light-activated metastable trap states of atomistic origin.[43,44] Experimental and theoretical characterizations suggest that localized charged states strongly couple to local structural lattice distortions and methylammonium (MA) quasistatic configurations. These small polarons seed the creation of macroscopic charged domains prohibiting efficient charge extraction. Since these initial studies, there has been additional evidence that polarons play a role in the charge carrier behavior in perovskite materials.[45−50] In the process of thermalization, the polaron phonon can reach equilibration by transferring thermal energy to the surrounding lattice, giving rise to a cooled charge carrier.[51] Small polarons are believed to be minority carriers that can lead to shifts in the near-infrared absorption edge, local structural distortions, as well as steep temperature dependent photodegradation in perovskite materials.[43] In order to reduce photodegradation, enhance the carriers' mobility, and boost photocurrent in perovskite materials, it is therefore highly desirable to find a way to control the dressed quasiparticles in terms of spatial delocalization and the binding energy to the lattice degrees of freedom. Indeed, the formation of small polarons in $MAPbI_3$ was initially traced to cooperative MA^+ rotation and volumetric lattice strain. This interpretation was consistent with lower polaron binding energies in $CsPbI_3$ for both electrons and holes and led to the hypothesis that $FAPbI_3$ would be the best pure material to alleviate the photodegradation.[44] Alloying Cs, FA, and MA shall inhibit both concerted dipolar rotations and charge induced volumetric strain and thus has the potential to further affect the small polarons spatial distribution and reduce its binding energy.[40,44] Notice that large polaron formation is also affected by alloying, leading to a slight enhancement of large polaron stabilization, because of Cs apolar character, not screening added charges.[51]

In this Letter, we utilize ab initio calculations to systematically investigate polaronic properties in a variety of mixed-cation hybrid perovskites. With respect to the Goldschmidt tolerance factor, mixtures of the three cations lead on average to suitable structural stability tolerances. An additional advantage of alloying is the local symmetry breaking that prevents cooperative charge trapping through "concerted" cation reconfigurations. A mixed triple cation could form a perovskite with almost constant band gaps. Our modeling shows that cation alloying significantly reduces the polaron binding energies for both electrons and holes compared to that in pure $MAPbI_3$. This can be traced to a prebreaking of the crystal symmetry. Electron polarons undergo Jahn−Teller (JT) distortions with the central apical bonds stretching 15−30% from their neutral geometry and the equatorial bonds remaining nearly the same. Hole polarons get the central octahedrons contracted uniformly by about 5%. Thus, the cation-mixing seems to effectively control both the structural and electronic properties so as to improve the material performance of halide perovskites.

Materials with an ABX_3 composition make different crystal structures, contingent upon the size and interaction of the A-cation and the corner-sharing BX_6 octahedra. The Goldschmidt tolerance (t) is a reliable empirical index to predict what structure is preferentially formed.[52] The Goldschmidt

DOI: 10.1021/acs.jpclett.9b01077
J. Phys. Chem. Lett. 2019, 10, 3516−3524

tolerance factor is calculated from the ionic radius of the atoms using the following expression

$$t = \frac{r_A + r_X}{\sqrt{2}(r_B + r_X)} \quad (1)$$

Where r_A is the radius of the A-cation, r_B is the radius of the B-cation, and r_X is the radius of the anion. In general, corner-sharing perovskites can be formed in the range of $0.8 < t < 1.0$.[53,54] Using the Pauling radii,[55] $Cs^+ = 1.69$, $Pb^{2+} = 1.22$, and $I^- = 2.16$, and reasonable values for MA^+ and FA^+ of 2.17 and 2.56, respectively,[56] we get that the tolerance factor for $CsPbI_3$ is 0.805, $MAPbI_3$ is 0.906, and $FAPbI_3$ is 0.987. To achieve the ideal black perovskite phase, t must be limited to the range of 0.9−1.0. $CsPbI_3$, with $t = 0.805$, is too small to sustain the large PbI framework and induces large octahedral tilting accompanied by local lattice distortions.[57] This observation is in line with the tremendous difficulty of fabricating stable $CsPbI_3$ perovskites at room temperature. With a tolerance factor close to 1, FA should adopt a nearly cubic lattice. However, because of the disordered states of FA cations in the cuboctahedral cages formed with the 12 nearest-neighbor I atoms,[58] the asymmetrical FA ions reside off-center in the PbI_6 octahedron, causing the formation of a hexagonal nonperovskite structure.[59] This suggests that the alloyed perovskites contain a suitable mixing of the three cations, which yields an optimal tolerance factor and improvement of the stability of the perovskite and photoactive phase, as already confirmed in experiments.[39,40]

The three pure perovskites, $APbI_3$ (A = Cs, MA, FA), have indeed optical absorption onsets at ∼1.73 (black phase),[60] 1.51 (tetragonal),[58] and 1.43 (cubic)[58] eV, respectively. The band gap red-shift from Cs to MA to FA is associated with decreasing octahedral tilting with increasing cation size.[56,61] $MAPbI_3$ doping with Cs and FA is not expected to significantly change octahedral tilting and is anticipated to marginally change the band gap.[62,63] At the HSE+SOC level of theory, pure periodic $MAPbI_3$ has a band gap of 1.01−1.17 eV.[44] At this same level of theory, we built a periodic trication model of $FA_{0.688}MA_{0.25}Cs_{0.063}PbI_3$ in the tetragonal phase containing 185 atoms to mimic the stoichiometric ratio ($FA_{0.7}MA_{0.25}Cs_{0.05}PbI_3$) explored in experiment.[40] We find this mixed-cation system has a band gap of 1.18 eV. This indicates that Cs and FA codoping does not heavily influence the band gaps of materials.

In order to describe the substitution effect on the charged species (i.e., polaron size and its binding energy), we subsequently constructed a series of mixed-cation isolated clusters (Figure 1a) based on a pure $MAPbI_3$ cluster where the MA cations are arranged in an anti-ferroelectric order along the diagonal direction (Figure 1a,b). Assessment of polaronic effects assumes optimization of geometries of neutral and charged clusters followed by calculations of energies at these configurations[44,64,65] (see Supporting Information (SI) and discussion below). These simulations were carried out using the Gaussian 16 software package[66] under the hybrid exchange-correlation CAM-B3LYP functional[67] in a polarizable solvent (see computational details in SI). As a result of the size of the system, the use of a hybrid functional, and the intentional use of a local basis set, it was not possible to include the spin orbit coupling (SOC) effects to these calculations. This limitation does add a few caveats to our results. The electron reorganization/polaron binding energies are overestimated because of the lack of inclusion of SOC. Previously, we have also observed that because of the degeneracy at the bottom of the conduction band in the absence of SOC, the estimated Jahn−Teller (JT) distortions and displacements are larger than those observed in experiment.[68] In spite of these limitations, general trends across the materials series are predicted correctly.

One important aspect of carrier self-trapping and spatial localization is symmetry breaking that may show itself in the activation of normally forbidden infrared modes.[64,65] Electron coupling to acoustic or polar optical phonons leads to different polaronic species in semiconductor lattices with well-defined point group symmetries.[44] Empirical Hamiltonians, like Holstein's,[65] are built to introduce a nonlinearity into Schrodinger's equation and provoke a bifurcation. A purely small polaron scenario related to totally symmetric local strain was presented in our previous manuscript.[44] The JT distortions in HP materials are important in small polaron formation of electrons and are discussed in this manuscript and other previous manuscripts.[68,69] The JT distortion is intimately linked to electronic degrees of freedom and is an important signature of small polaron formation.[69,70] Consequently, it manifests in removing an electronic degeneracy, opening a band gap, and favoring a particular electronic state.

Table 1 summarizes calculated changes in bond lengths and energies between neutral and charged clusters obtained by comparing their respective optimal geometries. As with previous results,[69] we find that the hole polaron bond lengths universally shrink by about 5% in all directions (Table 1). For the electron polaron in all the materials studied, the bond lengths of the four equatorial Pb−I bonds (l_{eq}) in the central octahedron remain almost unchanged. In contrast, the apical Pb−I bond lengths (l_{ap}) in the central octahedron increase by at least 23% for the pure materials with Cs (32%) > MA (25%) > FA (23%), reflecting the order of inherent symmetry. Markedly, the effect is notably reduced to about 15% for mixed-cation materials with a standard deviation of 1.11. Thus, although the local lattice symmetry is also broken by the formation of electron polarons in alloyed systems, it is suggested that they are less likely to be observed in these systems because of smaller geometrical changes.

Table 1. Change in Pb−I Equatorial (l_{eq}) and Apical Bond (l_{ap}) Lengths (in Å) of the Central Octahedron as Defined in Figure 1c as Well as Their Standard Deviations (σ) in Mixed Systems

	change in Pb−I bond length (%)		
	electron		hole
	l_{eq}	l_{ap}	both
$CsPbI_3$	2	32	−5
$MAPbI_3$	2	25	−5
$FAPbI_3$	−2	23	−6
model I	2	17	−5
model II	2	15	−5
model III	3	14	−5
model IV	2	16	−5
model V	2	15	−5
model VI	2	17	−5
σ	0.37	1.11	0

According to the standard Marcus theory,[71,72] we characterize polaronic properties with two relaxation energies, the sum of which is the reorganization energy (see Figure S1 and

DOI: 10.1021/acs.jpclett.9b01077
J. Phys. Chem. Lett. 2019, 10, 3516−3524

Computational Details section). The internal reorganization energy essentially quantifies the variation of the electronic energy as a result of the geometry changes when an electron is added or removed from the cluster. For simplicity, we assume that the neutral and charged parabolas of the diabatic energy curves have the same curvature (Figure S1). This assumes that the reorganization energies for the neutral and charged diabatic energy surfaces are identical. However, as already reported in several studies,[73−75] the two reorganization energies and by consequence the curvature of the neutral and the charged parabolas of the diabatic energy can be different (Figure 2a).

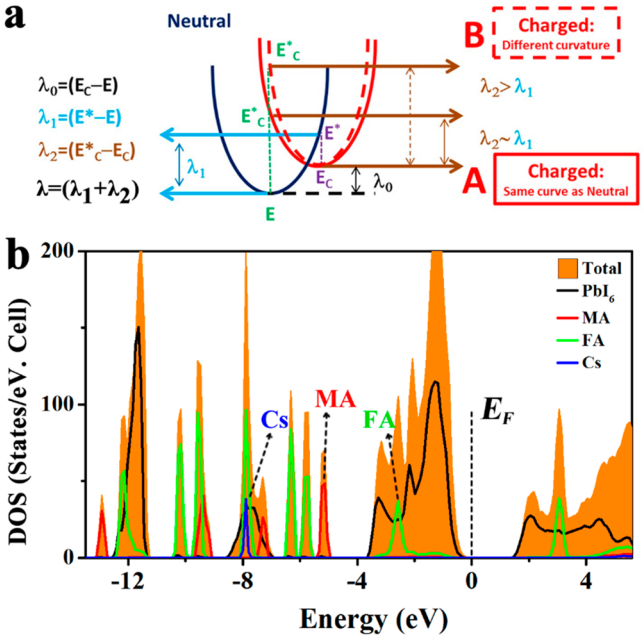

Figure 2. (a) Sketch of the three diabatic energy surfaces: neutral (dark blue), charged with the same curvature as neutral (type A, red), and charged with different from neutral curvature (type B, dash red). Type C is not shown for clarity ($\lambda_2 < \lambda_1$). (b) The computed projected DOS (pDOS) for a bulk trihalide system with a stoichiometric ratio of $Cs_{0.063}FA_{0.688}MA_{0.25}PbI_3$. Placement of the states of the valence band top for three cations are indicated by pink. The Fermi level is set to zero.

The polaron binding energy (E_{pol}) is then defined to be a half of the reorganization energy.[76] Generally, larger polaron binding energy reflects strong coupling of electronic system to the lattice (or electron−phonon coupling). In order to rationalize possible trends, we distinguish three cases: type A (same curve as neutral), B (different curvature with $\lambda_2 > \lambda_1$), and C (different curvature with $\lambda_2 < \lambda_1$). In fact, a majority of models for an electron-charged system are type B. CsFA−$MAPbI_3$ (model III) is a unique case where an almost type A case is calculated (Table 2). The situation is different for a hole-charged system. The near-type A is observed for four cases: $MAPbI_3$, 2Cs−$MAPbI_3$ (model IV), 2FA−$MAPbI_3$ (model V), and 2(CsFA)−$MAPbI_3$ (model VI). Type C, which is not observed for the electron-charged system case, appears for the hole-charged system in three cases: $CsPbI_3$, FA−$MAPbI_3$ (model II), and CsFA−$MAPbI_3$ (model III) clusters. Finally, type B arises only in two cases, $FAPbI_3$ and Cs−$MAPbI_3$ (model I) clusters. It is important to note that the list of cation alloying patterns is not exhaustive. Even though there are fluctuations in binding energy and delocalization, all

Table 2. Cavity Volumes (in Å^3), Reorganization Energies (λ, meV), and Polaron Binding Energies (E_{pol}, meV) Calculated for $CsPbI_3$, $MAPbI_3$, $FAPbI_3$, and Mixed-Cation Systems

		electron			hole		
models	volume	λ_1	λ_2	λ, E_{Pol}	λ_1	λ_2	λ, E_{Pol}
$CsPbI_3$	9993	724	918	1642, 821[a]	365	274	639, 320[a]
$MAPbI_3$	10 350	510	1377	1887, 944[a]	528	578	1106, 553[a]
$FAPbI_3$	10 708	536	723	1259, 630[a]	310	506	816, 408[a]
model I	10 322	525	677	1202, 601[a]	275	399	674, 337[a]
model II	10 350	545	621	1166, 583[a]	337	238	575, 288[a]
model III	10 335	541	572	1113, 557[a]	365	289	654, 327[a]
model IV	10 317	531	680	1211, 606[a]	284	313	597, 299[a]
model V	10 373	456	690	1146, 573[a]	290	301	591, 296[a]
model VI	10 388	474	638	1112, 556[a]	322	289	611, 306[a]

[a]Three types of diabatic energy surfaces (A, B, C) as defined within Marcus theory in Figure 2a.

alloys studied have an electron polaron binding energy smaller than that of any pure material. Likewise with holes, all alloys investigated have hole polaron binding energies smaller than those of $MAPbI_3$ and $FAPbI_3$. The alloys also uniformly show more delocalization than the pure materials.

Figure 3a,b shows an example of spatial distribution of electron−polaron spin density in $MAPbI_3$. Although both systems have −1 charge, the left and right plots show results obtained using the neutral and negatively charged optimal geometries, respectively. An increased spatial localization on the right image reflects lattice relaxation accommodating an addition of extra charge (self-trapping). As expected and previously reported,[69] the electron E_{pol} gets smaller once the A-site cation is changed from MA to Cs to FA (Table 2). This is rationalized by understanding that the MA system can stabilize a polaron via both volumetric strain and reorientation of the MA dipoles. Because both Cs and FA have vanishing or very small dipoles, only the former (local lattice strain) mechanism remains for charge stabilization in these cases.

According to our results, Cs and FA appear to be better at mitigating hole and electron polaron formation, respectively. The small size of the Cs cation allows its free motion inside the PbI_6 octahedron, which undergoes the largest JT distortion, and therefore leads to a larger electron polaron binding energy in the $CsPbI_3$ cluster compared to that in pure $FAPbI_3$. As discussed earlier, hole polaron formation causes uniform contraction of the surrounding lattice. In this case, having a very flexible lattice could allow for the material to "contort" itself to create a deep hole polaron. Recent experimental studies have found that FA has a near zero bulk modulus,[77] and we indeed find that the hole is not centrally located for the $FAPbI_3$ cluster in the neutral geometry (Figure 3c). The hole-charged system reveals noticeable nonsymmetric localization (Figure 3d) that has a binding energy almost as large as the $MAPbI_3$ cluster (Figure S3). In addition, we analyzed the projected density of states of a bulk trication perovskite $FA_{0.688}MA_{0.25}Cs_{0.063}PbI_3$ in the tetragonal phase (Figure 2b),

DOI: 10.1021/acs.jpclett.9b01077
J. Phys. Chem. Lett. 2019, 10, 3516−3524

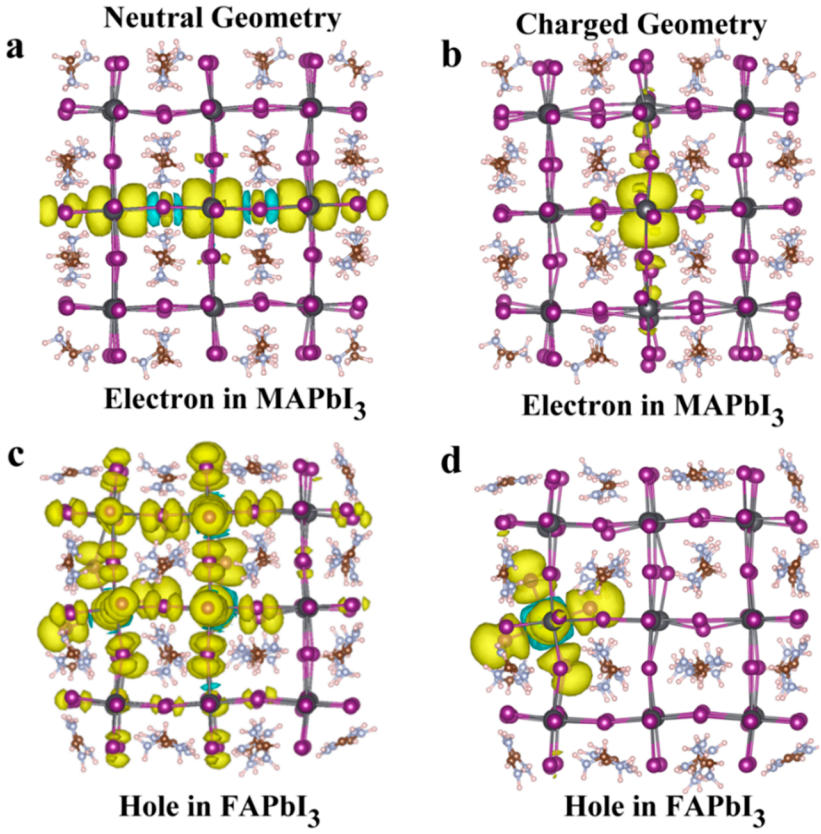

Figure 3. (a,b) Electron spin density distribution calculated using the optimal geometries of neutral and charged $MAPbI_3$ clusters, respectively. (c,d) The same as for (a,b) but for the hole spin density in $FAPbI_3$ clusters.

which has a similar stoichiometric ratio to the experimental system ($FA_{0.7}MA_{0.25}Cs_{0.05}PbI_3$).[40] Because FA states are significantly closer to the band edges, they are more likely to interact with the Pb−I lattice and contribute to the overall electron−phonon coupling compared to Cs or MA. Combining this with the fact that MA generates stabilization through both lattice distortion and dipole orientation, one can rationalize why hole polarons in pure $FAPbI_3$ are comparatively more localized compared to pure $CsPbI_3$ and have a spatial extent similar to their pure $MAPbI_3$ counterparts (see Figures S2−S4 for comparisons).

All alloyed clusters have lower electron−polaron binding energies compared to those of the pure clusters (Table 2). For example, calculated values are about half of what they are for pure $MAPbI_3$. For hole polarons, these alloyed systems have generally lower binding energies compared to the pure MA and FA systems with the exception of Cs−$MAPbI_3$: the latter has a polaron binding energy similar to that in the pure Cs system. Our simulations suggest that the systems with minimal electron and hole polaron binding energies are cosubstituted $MAPbI_3$ (models III and VI) and FA−$MAPbI_3$ (model II), respectively. The corresponding electron spin density distributions of model III are exemplified in Figure 4. These show slightly larger spatial extents, in good agreement with the corresponding quantities in Table 2. Spin density plots for all other alloys are shown in Figures S5−S9. Overall, compared to pristine $MAPbI_3$, we observe three general concomitant trends caused by alloying: reduced lattice distortion for electrons (Table 1), decreased polaron binding energies (Table 2), and increased spatial delocalization of the polaronic spin densities. In particular, we observe that both dipolar rotation and symmetric lattice distortions become smaller upon alloying. This can be rationalized by the fact that cosubstitutions with cations of different sizes lead to a slightly distorted and staggered lattice. Here, for instance, the cooperative motion of the remaining MA dipoles[40] neighboring the substituted cells will be disrupted, thus contributing to the reduction of polaron binding energy. This in turn ensures improved delocalization of the polaron spin densities, indicating that cation alloying effectively destabilizes small polarons and can potentially improve charge separation, diffusion, and collection in perovskite-based optoelectronic devices supporting experimental observations.[40]

Notably, we have been using a polarizable continuum model to account for the high dielectric constant environment of 3D halide perobkites. However, we recognize the fact that these clusters are perhaps closer to nanosystems with a large surface to volume ratio, and our calculations only account for the short-range distortions associated with small polarons owing to the small size of the isolated clusters. Subsequently, we may overestimate the polaronic contributions in terms of absolute numbers. To compensate for this effect, all the systems were chosen to have approximately the same size (∼2 nm), containing nearly 600 atoms, and thus were sufficiently large to approximate and mimic the bulk and fractional alloy effects. Larger clusters would be computationally intractable at the present time. Despite all of this, we expect observed trends to hold for 3D halide perovskite alloys. In addition, our calculations are static and provide just energetic estimates for reorganization energies. The dynamics of polaronic states in alloys is a very important question, where the theoretical simulation may complement experimental ultrafast measure-

DOI: 10.1021/acs.jpclett.9b01077
J. Phys. Chem. Lett. 2019, 10, 3516−3524

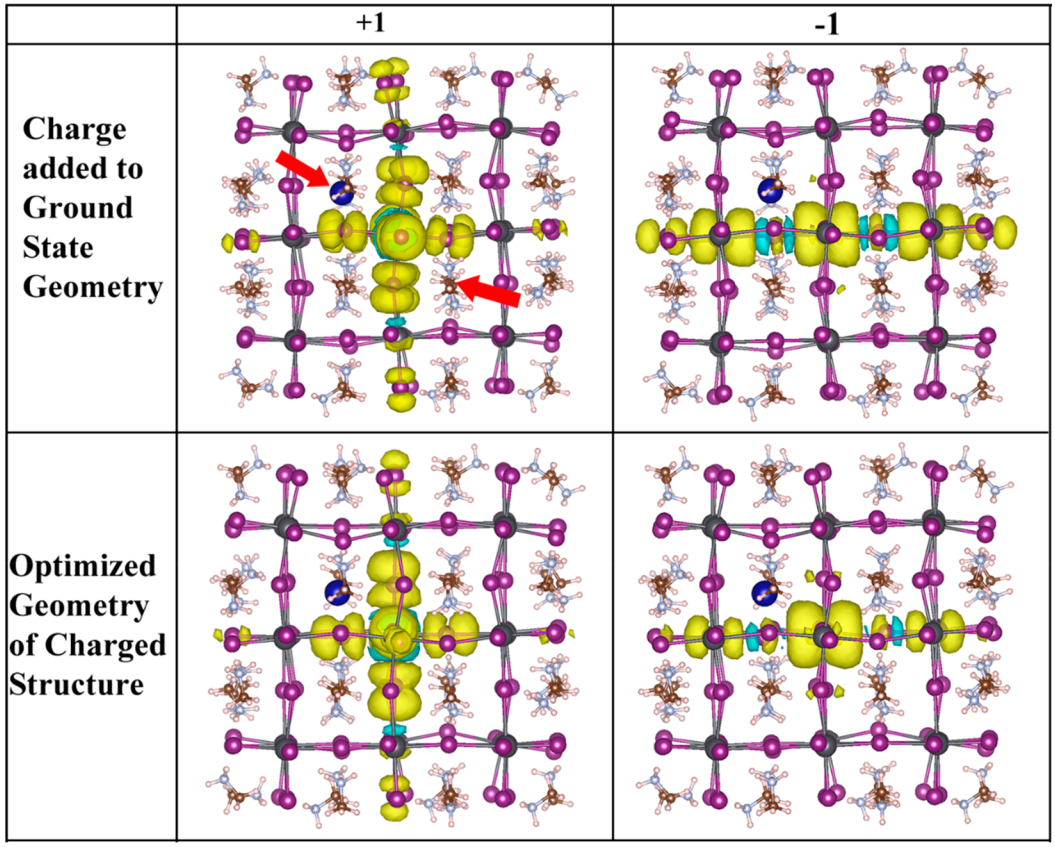

Figure 4. Calculated hole (left) and electron (right) spin density distribution of optimized neutral (top) and charged (bottom) CsFA–$MAPbI_3$ clusters (model III). The substituting Cs and FA are indicated by red arrows.

ments. For example such studies were done for $MAPI_3$ to link exciton–polaron dynamics with lattice displacements.[43] The NAMD simulations on polaron population using nonadiabatic molecular dynamics in alloys are ongoing.

In conclusion, we perform first principle calculations to investigate how alloying the A-site cation in $APbI_3$ halide perovskites influences structural stability, optical properties, and polaron binding energy. Our cluster models show that cation alloying significantly reduces the binding energies of small polarons for both electrons and holes roughly by a factor of 2 compared to pure $MAPbI_3$ and to a lesser extent compared to $CsPbI_3$ and $FAPbI_3$. Observed trends are rationalized by the prebreaking of the crystal symmetry that prevents concerted MA motion toward stabilization of a tightly bound polaron and ultimately causes the polarons to be more spatially delocalized. The electron polarons undergo JT distortions with the central apical bonds stretching 15–30% from their neutral geometry and the equatorial bonds remaining nearly the same. The more symmetric pure materials undergo stronger JT distortions and larger polaron binding energies. On the other hand, in all studied systems, the Pb–I bonds in the central octahedrons of hole polarons uniformly shrink by about 5%. This difference in behavior could be utilized to determine which type of particle (electron or hole) is localized by a polaronic effect. In addition, alloying does not change significantly the band gap. Thus, our simulations show that a polaron binding energy can be tuned via Cs, FA, and MA alloying, rationalizing recent experimental reports.[40] Our calculations are static and provide energetic estimates for reorganization energies. The dynamics of polaronic states may complement experimental ultrafast measurements. Overall, our computational results provide detailed analysis of mechanisms of lattice distortions because of the presence of a localized charge carrier guiding experiments toward more stable halide perovskite-based materials with improved optoelectronic performance.

■ ASSOCIATED CONTENT

Supporting Information

The Supporting Information is available free of charge on the ACS Publications website at DOI: 10.1021/acs.jpclett.9b01077.

Computational details; schematic depiction of the potential energy surfaces of the neutral and charged clusters; hole and electron spin density distributions for pure and cation-alloyed $MAPbI_3$ clusters (PDF)

■ AUTHOR INFORMATION

Corresponding Authors

*E-mail: liujiang86@gmail.com. (L.Z.)
*E-mail: ajneukirch@lanl.gov. (A.J.N.)

ORCID

Liujiang Zhou: 0000-0001-5814-4486
Claudine Katan: 0000-0002-2017-5823
Laurent Pedesseau: 0000-0001-9414-8644
Jacky Even: 0000-0002-4607-3390
Aditya D. Mohite: 0000-0001-8865-409X
Sergei Tretiak: 0000-0001-5547-3647
Amanda J. Neukirch: 0000-0002-6583-0086

DOI: 10.1021/acs.jpclett.9b01077
J. Phys. Chem. Lett. 2019, 10, 3516–3524

Notes

The authors declare no competing financial interest.

■ ACKNOWLEDGMENTS

The work at Los Alamos National Laboratory (LANL) was supported by the LANL LDRD program (A.J.N., I.A., L.Z., W.N, H.T., J.J.C., and S.T.). This work was done in part at the Center for Nonlinear Studies (CNLS) and the Center for Integrated Nanotechnologies CINT), a U.S. Department of Energy and Office of Basic Energy Sciences user facility, at LANL. This research used resources provided by the LANL Institutional Computing Program. Los Alamos National Laboratory is operated by Triad National Security, LLC, for the National Nuclear Security Administration of the U.S. Department of Energy (Contract No. 89233218NCA000001). The work in France was supported by Agence Nationale pour la Recherche (TRANSHYPERO project). J.E. acknowledges financial support from the Institut Universitaire de France. A.D.M. acknowledges the DOE-EERE 0001647-1544 grant for this work. A.J.N. would like to thank Mikael Kepenekian for useful insight and discussion on the set up of the calculations.

■ REFERENCES

(1) Manser, J. S.; Christians, J. A.; Kamat, P. V. Intriguing Optoelectronic Properties of Metal Halide Perovskites. *Chem. Rev.* **2016**, *116*, 12956−13008.

(2) Saparov, B.; Mitzi, D. B. Organic−Inorganic Perovskites: Structural Versatility for Functional Materials Design. *Chem. Rev.* **2016**, *116*, 4558−4596.

(3) Yamada, Y.; Nakamura, T.; Endo, M.; Wakamiya, A.; Kanemitsu, Y. Near-Band-Edge Optical Responses of Solution-Processed Organic−Inorganic Hybrid Perovskite CH3NH3PbI3 on Mesoporous TiO2 Electrodes. *Appl. Phys. Express* **2014**, *7*, 032302.

(4) Chiang, C.-H.; Wu, C.-G. A Method for the Preparation of Highly Oriented MAPbI3 Crystallites for High-Efficiency Perovskite Solar Cells to Achieve an 86% Fill Factor. *ACS Nano* **2018**, *12*, 10355−10364.

(5) Wang, J.; Wang, N.; Jin, Y.; Si, J.; Tan, Z.; Du, H.; Cheng, L.; Dai, X.; Bai, S.; He, H.; et al. Interfacial Control Toward Efficient and Low-Voltage Perovskite Light-Emitting Diodes. *Adv. Mater.* **2015**, *27*, 2311−2316.

(6) Yuan, M.; Quan, L. N.; Comin, R.; Walters, G.; Sabatini, R.; Voznyy, O.; Hoogland, S.; Zhao, Y.; Beauregard, E. M.; Kanjanaboos, P.; et al. Perovskite Energy Funnels for Efficient Light-Emitting Diodes. *Nat. Nanotechnol.* **2016**, *11*, 872−877.

(7) Luo, J.; Im, J.-H.; Mayer, M. T.; Schreier, M.; Nazeeruddin, M. K.; Park, N.-G.; Tilley, S. D.; Fan, H. J.; Gratzel, M. Water Photolysis at 12.3% Efficiency via Perovskite Photovoltaics and Earth-Abundant Catalysts. *Science (Washington, DC, U. S.)* **2014**, *345*, 1593−1596.

(8) Yakunin, S.; Sytnyk, M.; Kriegner, D.; Shrestha, S.; Richter, M.; Matt, G. J.; Azimi, H.; Brabec, C. J.; Stangl, J.; Kovalenko, M. V.; et al. Detection of X-Ray Photons by Solution-Processed Lead Halide Perovskites. *Nat. Photonics* **2015**, *9*, 444−U44.

(9) Yakunin, S.; Dirin, D. N.; Shynkarenko, Y.; Morad, V.; Cherniukh, I.; Nazarenko, O.; Kreil, D.; Nauser, T.; Kovalenko, M. Detection of Gamma Photons Using Solution-Grown Single Crystals of Hybrid Lead Halide Perovskites. *Nat. Photonics* **2016**, *10*, 585−589.

(10) Kepenekian, M.; Robles, R.; Katan, C.; Sapori, D.; Pedesseau, L.; Even, J. Rashba and Dresselhaus Effects in Hybrid Organic-Inorganic Perovskites: From Basics to Devices. *ACS Nano* **2015**, *9*, 11557−11567.

(11) Muthu, C.; Nagamma, S. R.; Nair, V. C. Luminescent Hybrid Perovskite Nanoparticles as a New Platform for Selective Detection of 2,4,6-Trinitrophenol. *RSC Adv.* **2014**, *4*, 55908−55911.

(12) Stranks, S. D.; Snaith, H. J. Metal-Halide Perovskites for Photovoltaic and Light-Emitting Devices. *Nat. Nanotechnol.* **2015**, *10*, 391−402.

(13) Pellet, N.; Gao, P.; Gregori, G.; Yang, T.-Y.; Nazeeruddin, M. K.; Maier, J.; Grätzel, M. Mixed-Organic-Cation Perovskite Photovoltaics for Enhanced Solar-Light Harvesting. *Angew. Chem., Int. Ed.* **2014**, *53*, 3151−3157.

(14) Hodes, G. Perovskite-Based Solar Cells. *Science (Washington, DC, U. S.)* **2013**, *342*, 317−318.

(15) Niu, G.; Guo, X.; Wang, L. Review of Recent Progress in Chemical Stability of Perovskite Solar Cells. *J. Mater. Chem. A* **2015**, *3*, 8970−8980.

(16) Li, X.; Tschumi, M.; Han, H.; Babkair, S.; Alzubaydi, A.; Ansari, A. A.; Habib, S. S.; Nazeeruddin, M. K.; Zakeeruddin, S. M.; Grätzel, M. Outdoor Performance and Stability under Elevated Temperatures and Long-Term Light Soaking of Triple-Layer Mesoporous Perovskite Photovoltaics. *Energy Technol.* **2015**, *3*, 551−555.

(17) Grätzel, M. The Light and Shade of Perovskite Solar Cells. *Nat. Mater.* **2014**, *13*, 838−842.

(18) Tsai, H.; Nie, W.; Blancon, J.-C.; Stoumpos, C. C.; Asadpour, R.; Harutyunyan, B.; Neukirch, A. J.; Verduzco, R.; Crochet, J. J.; Tretiak, S.; et al. High-Efficiency Two-Dimensional Ruddlesden−Popper Perovskite Solar Cells. *Nature* **2016**, *536*, 312−316.

(19) Chen, Z.; Zhang, C.; Jiang, X.-F.; Liu, M.; Xia, R.; Shi, T.; Chen, D.; Xue, Q.; Zhao, Y.-J.; Su, S.; et al. High-Performance Color-Tunable Perovskite Light Emitting Devices through Structural Modulation from Bulk to Layered Film. *Adv. Mater.* **2017**, *29*, 1603157.

(20) Ono, L. K.; Juarez-Perez, E. J.; Qi, Y. Progress on Perovskite Materials and Solar Cells with Mixed Cations and Halide Anions. *ACS Appl. Mater. Interfaces* **2017**, *9*, 30197−30246.

(21) Correa-Baena, J.-P.; Abate, A.; Saliba, M.; Tress, W.; Jacobsson, T. J.; Grätzel, M.; Hagfeldt, A. The Rapid Evolution of Highly Efficient Perovskite Solar Cells. *Energy Environ. Sci.* **2017**, *10*, 710−727.

(22) Ngo, T. T.; Suarez, I.; Antonicelli, G.; Cortizo-Lacalle, D.; Martinez-Pastor, J. P.; Mateo-Alonso, A.; Mora-Sero, I. Enhancement of the Performance of Perovskite Solar Cells, LEDs, and Optical Amplifiers by Anti-Solvent Additive Deposition. *Adv. Mater.* **2017**, *29*, 1604056.

(23) Barker, A. J.; Sadhanala, A.; Deschler, F.; Gandini, M.; Senanayak, S. P.; Pearce, P. M.; Mosconi, E.; Pearson, A. J.; Wu, Y.; Srimath Kandada, A. R.; et al. Defect-Assisted Photoinduced Halide Segregation in Mixed-Halide Perovskite Thin Films. *ACS Energy Lett.* **2017**, *2*, 1416−1424.

(24) Noh, J. H.; Im, S. H.; Heo, J. J.; Mandal, T. N.; Seok, S. Il. Chemical Management for Colorful, Efficient, and Stable Inorganic-Organic Hybrid Nanostructured Solar Cells. *Nano Lett.* **2013**, *13*, 1764−1769.

(25) Lee, J.-W.; Kim, D.-H.; Kim, H.-S.; Seo, S.-W.; Cho, S. M.; Park, N.-G. Formamidinium and Cesium Hybridization for Photo- and Moisture-Stable Perovskite Solar Cell. *Adv. Energy Mater.* **2015**, *5*, 1501310.

(26) Eperon, G. E.; Stranks, S. D.; Menelaou, C.; Johnston, M. B.; Herz, L. M.; Snaith, H. J. Formamidinium Lead Trihalide: A Broadly Tunable Perovskite for Efficient Planar Heterojunction Solar Cells. *Energy Environ. Sci.* **2014**, *7*, 982−988.

(27) Stoumpos, C. C.; Malliakas, C. D.; Kanatzidis, M. G. Semiconducting Tin and Lead Iodide Perovskites with Organic Cations: Phase Transitions, High Mobilities, and near-Infrared Photoluminescent Properties. *Inorg. Chem.* **2013**, *52*, 9019−9038.

(28) Conings, B.; Drijkoningen, J.; Gauquelin, N.; Babayigit, A.; D'Haen, J.; D'Olieslaeger, L.; Ethirajan, A.; Verbeeck, J.; Manca, J.; Mosconi, E.; et al. Intrinsic Thermal Instability of Methylammonium Lead Trihalide Perovskite. *Adv. Energy Mater.* **2015**, *5*, 1500477.

(29) Protesescu, L.; Yakunin, S.; Bodnarchuk, M. I.; Krieg, F.; Caputo, R.; Hendon, C. H.; Yang, R. X.; Walsh, A.; Kovalenko, M. V. Nanocrystals of Cesium Lead Halide Perovskites CsPbI3, (X = Cl, Br, and I): Novel Optoelectronic Materials Showing Bright Emission with Wide Color Gamut. *Nano Lett.* **2015**, *15*, 3692−3696.

(30) Sutton, R. J.; Eperon, G. E.; Miranda, L.; Parrott, E. S.; Kamino, B. A.; Patel, J. B.; Hörantner, M. T.; Johnston, M. B.; Haghighirad, A.

DOI: 10.1021/acs.jpclett.9b01077
J. Phys. Chem. Lett. 2019, 10, 3516−3524

A.; Moore, D. T.; et al. Bandgap-Tunable Cesium Lead Halide Perovskites with High Thermal Stability for Efficient Solar Cells. *Adv. Energy Mater.* **2016**, *6*, 1502458.
(31) Eperon, G. E.; Paternò, G. M.; Sutton, R. J.; Zampetti, A.; Haghighirad, A. A.; Cacialli, F.; Snaith, H. J. Inorganic Caesium Lead Iodide Perovskite Solar Cells. *J. Mater. Chem. A* **2015**, *3*, 19688−19695.
(32) Yamada, K.; Nishikubo, R.; Oga, H.; Ogomi, Y.; Hayase, S.; Kanno, S.; Imamura, Y.; Hada, M.; Saeki, A. Anomalous Dielectric Behavior of a Pb/Sn Perovskite: Effect of Trapped Charges on Complex Photoconductivity. *ACS Photonics* **2018**, *5*, 3189.
(33) Kulbak, M.; Cahen, D.; Hodes, G. How Important Is the Organic Part of Lead Halide Perovskite Photovoltaic Cells? Efficient CsPbBr3 Cells. *J. Phys. Chem. Lett.* **2015**, *6*, 2452−2456.
(34) Marronnier, A.; Roma, G.; Boyer-Richard, S.; Pedesseau, L.; Jancu, J.-M.; Bonnassieux, Y.; Katan, C.; Stoumpos, C. C.; Kanatzidis, M. G.; Even, J. Anharmonicity and Disorder in the Black Phases of Cesium Lead Iodide Used for Stable Inorganic Perovskite Solar Cells. *ACS Nano* **2018**, *12*, 3477−3486.
(35) Yi, C.; Luo, J.; Meloni, S.; Boziki, A.; Ashari-Astani, N.; Grätzel, C.; Zakeeruddin, S. M.; Röthlisberger, U.; Grätzel, M. Entropic Stabilization of Mixed A-Cation ABX3Metal Halide Perovskites for High Performance Perovskite Solar Cells. *Energy Environ. Sci.* **2016**, *9*, 656−662.
(36) McMeekin, D. P.; Sadoughi, G.; Rehman, W.; Eperon, G. E.; Saliba, M.; Hörantner, M. T.; Haghighirad, A.; Sakai, N.; Korte, L.; Rech, B.; et al. A Mixed-Cation Lead Mixed-Halide Perovskite Absorber for Tandem Solar Cells. *Science (Washington, DC, U. S.)* **2016**, *351*, 151−155.
(37) Yi, C.; Li, X.; Luo, J.; Zakeeruddin, S. M.; Grätzel, M. Perovskite Photovoltaics with Outstanding Performance Produced by Chemical Conversion of Bilayer Mesostructured Lead Halide/TiO2 Films. *Adv. Mater.* **2016**, *28*, 2964−2970.
(38) Saliba, M.; Matsui, T.; Domanski, K.; Seo, J.-Y.; Ummadisingu, A.; Zakeeruddin, S. M.; Correa-Baena, J.-P.; Tress, W. R.; Abate, A.; Hagfeldt, A.; et al. Incorporation of Rubidium Cations Into Perovskite Solar Cells Improves Photovoltaic Performance. *Science (Washington, DC, U. S.)* **2016**, *354*, 206−209.
(39) Saliba, M.; Matsui, T.; Seo, J.-Y.; Domanski, K.; Correa-Baena, J.-P.; Nazeeruddin, M. K.; Zakeeruddin, S. M.; Tress, W.; Abate, A.; Hagfeldt, A.; et al. Cesium-Containing Triple Cation Perovskite Solar Cells: Improved Stability, Reproducibility and High Efficiency. *Energy Environ. Sci.* **2016**, *9*, 1989−1997.
(40) Tsai, H.; Asadpour, R.; Blancon, J.-C.; Stoumpos, C. C.; Durand, O.; Strzalka, J. W.; Chen, B.; Verduzco, R.; Ajayan, P. M.; Tretiak, S.; et al. Light-Induced Lattice Expansion Leads to High-Efficiency Perovskite Solar Cells. *Science (Washington, DC, U. S.)* **2018**, *360*, 67−70.
(41) Jeon, N. J.; Noh, J. H.; Yang, W. S.; Kim, Y. C.; Ryu, S.; Seo, J.; Seok, S. Il. Compositional Engineering of Perovskite Materials for High-Performance Solar Cells. *Nature* **2015**, *517*, 476−480.
(42) Binek, A.; Hanusch, F. C.; Docampo, P.; Bein, T. Stabilization of the Trigonal High-Temperature Phase of Formamidinium Lead Iodide. *J. Phys. Chem. Lett.* **2015**, *6*, 1249−1253.
(43) Nie, W.; Blancon, J.; Neukirch, A. J.; Appavoo, K.; Tsai, H.; Chhowalla, M.; Alam, M. A.; Sfeir, M. Y.; Katan, C.; Even, J.; et al. Light-Activated Photocurrent Degradation and Self-Healing in Perovskite Solar Cells. *Nat. Commun.* **2016**, *7*, 11574.
(44) Neukirch, A. J.; Nie, W.; Blancon, J.-C.; Appavoo, K.; Tsai, H.; Sfeir, M. Y.; Katan, C.; Even, J.; Crochet, J. J.; Gupta, G.; et al. Polaron Stabilization by Cooperative Lattice and Cation Rotations in Hybrid Perovskite Materials. *Nano Lett.* **2016**, *16*, 3809−3816.
(45) Thouin, F.; Valverde-Chávez, D. A.; Quarti, C.; Cortecchia, D.; Bargigia, I.; Beljonne, D.; Petrozza, A.; Silva, C.; Srimath Kandada, A. R. Phonon Coherences Reveal the Polaronic Character of Excitons in Two-Dimensional Lead Halide Perovskites. *Nat. Mater.* **2019**, *18*, 349.
(46) Zheng, K.; Abdellah, M.; Zhu, Q.; Kong, Q.; Jennings, G.; Kurtz, C. A.; Messing, M. E.; Niu, Y.; Gosztola, D. J.; Al-marri, M. J.; et al. Direct Experimental Evidence for Photoinduced Strong-Coupling Polarons in Organolead Halide Perovskite Nanoparticles. *J. Phys. Chem. Lett.* **2016**, *7*, 4535−4539.
(47) Zhu, H.; Miyata, K.; Fu, Y.; Wang, J.; Joshi, P. P.; Niesner, D.; Williams, K. W.; Jin, S.; Zhu, X.-Y. Screening in Crystalline Liquids Protects Energetic Carriers in Hybrid Perovskites. *Science (Washington, DC, U. S.)* **2016**, *353*, 1409−1413.
(48) Miyata, K.; Atallah, T. L.; Zhu, X.-Y. Lead Halide Perovskites: Crystal-Liquid Duality, Phonon Glass Electron Crystals, and Large Polaron Formation. *Sci. Adv.* **2017**, *3*, No. e1701469.
(49) Yin, J.; Li, H.; Cortecchia, D.; Soci, C.; Bredas, J. Excitonic and Polaronic Properties of 2D Hybrid Organic − Inorganic Perovskites. *ACS Energy Lett.* **2017**, *2*, 417−423.
(50) Mccall, K. M.; Stoumpos, C. C.; Kostina, S. S.; Kanatzidis, M. G.; Wessels, B. W. Strong Electron − Phonon Coupling and Self-Trapped Excitons in the Defect Halide Perovskites $A_3M_2I_9$ (A = Cs, Rb ; M = Bi, Sb). *Chem. Mater.* **2017**, *29*, 4129−4145.
(51) Mahata, A.; Meggiolaro, D.; De Angelis, F. From Large to Small Polarons in Lead, Tin, and Mixed Lead−Tin Halide Perovskites. *J. Phys. Chem. Lett.* **2019**, *10*, 1790−1798.
(52) Goldschmidt, V. M. Die Gesetze Der Krystallochemie. *Naturwissenschaften* **1926**, *14*, 477−485.
(53) Li, C.; Soh, K. C. K.; Wu, P. Fromability of ABO3 Perovskites. *J. Alloys Compd.* **2004**, *372*, 40−48.
(54) Li, C.; Lu, X.; Ding, W.; Feng, L.; Gao, Y.; Guo, Z. Formability of ABX3 (X + F, Cl, Br, I) Halide Perovskites. *Acta Crystallogr., Sect. B: Struct. Sci.* **2008**, *64*, 702−707.
(55) Sun, Q.; Yin, W. Thermodynamic Stability Trend of Cubic Perovskites. *J. Am. Chem. Soc.* **2017**, *139*, 14905−14908.
(56) Amat, A.; Mosconi, E.; Ronca, E.; Quarti, C.; Umari, P.; Nazeeruddin, M. K.; Grätzel, M.; De Angelis, F. Cation-Induced Band-Gap Tuning in Organohalide Perovskites: Interplay of Spin−Orbit Coupling and Octahedra Tilting. *Nano Lett.* **2014**, *14*, 3608−3616.
(57) Luo, P.; Zhou, S.; Zhou, Y.; Xia, W.; Sun, L.; Cheng, J.; Xu, C.; Lu, Y. Fabrication of CsxFA1−XPbI3Mixed-Cation Perovskites via Gas-Phase-Assisted Compositional Modulation for Efficient and Stable Photovoltaic Devices. *ACS Appl. Mater. Interfaces* **2017**, *9*, 42708−42716.
(58) Pang, S.; Hu, H.; Zhang, J.; Lv, S.; Yu, Y.; Wei, F.; Qin, T.; Xu, H.; Liu, Z.; Cui, G. NH2CH═NH2PbI3: An Alternative Organolead Iodide Perovskite Sensitizer for Mesoscopic Solar Cells. *Chem. Mater.* **2014**, *26*, 1485−1491.
(59) Chen, Q.; De Marco, N.; Yang, Y.; Song, T.-B.; Chen, C.-C.; Zhao, H.; Hong, Z.; Zhou, H.; Yang, Y. Under the Spotlight: The Organic−Inorganic Hybrid Halide Perovskite for Optoelectronic Applications. *Nano Today* **2015**, *10*, 355−396.
(60) Eperon, G. E.; Stranks, S. D.; Menelaou, C.; Johnston, M. B.; Herz, L. M.; Snaith, H. J. Formamidinium Lead Trihalide: A Broadly Tunable Perovskite for Efficient Planar Heterojunction Solar Cells. *Energy Environ. Sci.* **2014**, *7*, 982−988.
(61) Pedesseau, L.; Sapori, D.; Traore, B.; Robles, R.; Fang, H.-H.; Loi, M. A.; Tsai, H.; Nie, W.; Blancon, J.-C.; Neukirch, A.; et al. Advances and Promises of Layered Halide Hybrid Perovskite Semiconductors. *ACS Nano* **2016**, *10*, 9776−9786.
(62) Niu, G.; Li, W.; Li, J.; Liang, X.; Wang, L. Enhancement of Thermal Stability for Perovskite Solar Cells through Cesium Doping. *RSC Adv.* **2017**, *7*, 17473−17479.
(63) Bella, F.; Renzi, P.; Cavallo, C.; Gerbaldi, C. Caesium for Perovskite Solar Cells: An Overview. *Chem. - Eur. J.* **2018**, *24*, 12183−12205.
(64) Zuppiroli, L.; Bieber, A.; Michoud, D.; Galli, G.; Gygi, F.; Bussac, M.; Andre, J. Polaron Formation and Symmetry Breaking. *Chem. Phys. Lett.* **2003**, *374*, 7−12.
(65) Holstein, T. Studis of Polaron Motion: Part II. The "Small" Polaron. *Ann. Phys. (Amsterdam, Neth.)* **1959**, *8*, 343−389.
(66) Frisch, M. J.; Trucks, G. W.; Schlegel, H. B.; Scuseria, G. E.; Robb, M. A.; Cheeseman, J. R.; Scalmani, G.; Barone, V.; Petersson, G. A.; Nakatsuji, H.; Li, X.; Caricato, M.; Marenich, A. V.; Blolino, J.;

DOI: 10.1021/acs.jpclett.9b01077
J. Phys. Chem. Lett. 2019, 10, 3516−3524

Janesko, B. G.; Gomperts, R.; Mennucci, B.; Hratchian, H. P.; Ortiz, J. V.; Izmaylov, A. F.; Sonnenberg, J. L.; Williams-Young, D.; Ding, F.; Lipparini, F.; Egidi, F.; Goings, J.; Peng, B.; Petrone, A.; Henderson, T.; Ranasinghe, D.; Zakrzewski, V. G.; Gao, J.; Rega, N.; Zheng, G.; Liang, W.; Hada, M.; Ehara, M.; Toyota, K.; Fukuda, R.; Hasegawa, J.; Ishida, M.; Nakajima, T.; Honda, Y.; Kitao, O.; Nakai, H.; Vreven, T.; Throssell, K.; Montgomery, J. A., Jr.; Peralta, J. E.; Oligaro, F.; Bearpark, M. J.; Heyd, J. J; Brothers, E. N.; Kudin, K. N.; Staroverov, V. N.; Keith, T. A.; Kobayashi, R.; Normand, J.; Ragavachari, K.; Rendell, A. P.; Burant, J. C.; Iyengar, S. S.; Tomasi, J.; Cossi, M.; Millam, J. M.; Klene, M.; Adamo, C.; Cammi, R.; Ochterski, J. W.; Martin, R. L.; Morokuma, K.; Farkas, O.; Foresman, J. B.; Fox, D. J. *Gaussian 16*, revision B.01; Gaussian, Inc.: Wallingford, CT, 2016.

(67) Yanai, T.; Tew, D. P.; Handy, N. C. A New Hybrid Exchange–Correlation Functional Using the Coulomb-Attenuating Method (CAM-B3LYP). *Chem. Phys. Lett.* **2004**, *393*, 51–57.

(68) Park, M.; Neukirch, A. J.; Reyes-Lillo, S. E.; Lai, M.; Ellis, S. R.; Dietze, D.; Neaton, J. B.; Yang, P.; Tretiak, S.; Mathies, R. A. Excited-State Vibrational Dynamics Toward the Polaron in Methylammonium Lead Iodide Perovskite. *Nat. Commun.* **2018**, *9*, 2525.

(69) Neukirch, A. J.; Abate, I. I.; Zhou, Li.; Nie, W.; Tsai, H.; Pedesseau, L.; Even, J.; Crochet, J. J.; Mohite, A. J.; Katan, C.; et al. Geometry Distortion and Small Polaron Binding Energy Changes with Ionic Substitution in Halide Perovskites. *J. Phys. Chem. Lett.* **2018**, *9*, 7130–7136.

(70) Varignon, J.; Bristowe, N. C.; Ghosez, P. Electric Field Control of Jahn-Teller Distortions in Bulk Perovskites. *Phys. Rev. Lett.* **2016**, *116*, 057602.

(71) Marcus, R. A. On the Theory of Oxidation-Reduction Reactions Involving Electron Transfer. II. Applications to Data on the Rates of Isotopic Exchange Reactions. *J. Chem. Phys.* **1957**, *26*, 867–871.

(72) Marcus, R. A. Electron Transfer Reactions in Chemistry: Theory and Experiment (Nobel Lecture). *Angew. Chem., Int. Ed. Engl.* **1993**, *32*, 1111–1121.

(73) Yang, D. Y.; Cukier, R. I. The Transition from Nonadiabatic to Solvent Controlled Adiabatic Electron Transfer: Solvent Dynamical Effects in the Inverted Regime. *J. Chem. Phys.* **1989**, *91*, 281–292.

(74) Tang, J. Electron-Transfer Reactions Involving Non-Linear Spin-Boson Interactions. *Chem. Phys.* **1994**, *188*, 143–160.

(75) Denk, C.; Morillo, M.; Sánchez-Burgos, F.; Sánchez, A. Reorganization Energies for Charge Transfer Reactions in Binary Mixtures of Dipolar Hard Sphere Solvents: A Monte Carlo Study. *J. Chem. Phys.* **1999**, *110*, 473–483.

(76) Coropceanu, V.; Cornil, J.; da Silva Filho, D. A.; Olivier, Y.; Silbey, R.; Brédas, J.-L. Charge Transport in Organic Semiconductors. *Chem. Rev.* **2007**, *107*, 926–952.

(77) Ferreira, A. C.; Létoublon, A.; Paofai, S.; Raymond, S.; Ecolivet, C.; Rufflé, B.; Cordier, S.; Katan, C.; Saidaminov, M. I.; Zhumekenov, A. A.; et al. Elastic Softness of Hybrid Lead Halide Perovskites. *Phys. Rev. Lett.* **2018**, *121*, 085502.

DOI: 10.1021/acs.jpclett.9b01077
J. Phys. Chem. Lett. 2019, 10, 3516–3524